Computers and Geosciences 124 (2019) 14–26

Contents lists available at ScienceDirect

Computers and Geosciences

journal homepage: www.elsevier.com/locate/cageo

Semi-automated procedure of digitalization and study of rock thin section porosity applying optical image analysis tools☆

Edgar Berrezueta[a,*], María José Domínguez-Cuesta[b], Ángel Rodríguez-Rey[b]

[a] Instituto Geológico y Minero de España (IGME), C/Matemático Pedrayes 25, Oviedo, 33005, Spain
[b] Universidad de Oviedo, Departamento de Geología, C/Jesús Arias de Velasco s/n, Oviedo, 33005, Spain

ARTICLE INFO

Keywords:
High-resolution scanner
Optical image analysis
GIS
Porosity
Virtual microscopy

ABSTRACT

A detailed description of a semi-automated process of digitalization, visualization and quantification of rock thin sections by applying Optical Image Analysis (OIA) is presented. The main goal of this process is to guarantee the reproducibility of the OIA method on images acquired by a high-resolution scanner (HRS, *Cannon V850 Pro*) from thin sections, emulating an optical microscope. The method consists of the following sequence of operations and functions: i) image acquisition under polarized conditions by image analysis programs (*SilverFast SE Plus 8I*), ii) spatial correction of images to ensure correct spatial correlation and registration by using a Geographic Information System software (*QGIS* 2.14.0-Essen), iii) pore identification and pore size and shape parameter quantification (*ImageJ 1.50i*), iv) storage of the high resolution polarized images. This semi-automated process grants effective pore segmentation based on images of different cross-polarized light conditions (90°/0°; 135°/45°) and plane-polarized light conditions (90°/-; 0°/-) of the same petrographic scene. The optical resolution of the used images (6400 dots per inch) enables the visualization of pores with diameters ranging from 3.97 μm to 2000 μm. The proposed method was applied to and tested by the quantification of optical pores of two sedimentary rocks before and after their exposure to supercritical CO_2 (t: 970 h). Through this process, rock pore evolution after interaction with supercritical CO_2 can be correctly assessed. The applied OIA system and, in particular, the sets of obtained high resolution polarized digital images provided a basis for the development of a remote visualization system. This system makes it possible to virtually represent thin sections similarly to a simple virtual microscope. The described workflow offers a fast, effective and reproducible methodology that could complement petrographic studies.

1. Introduction and objectives

Identification and quantification of mineral phases, textures and porosity by optical image analysis (OIA) represents an important contribution to the standard petrographic characterization using optical microscopy (Arena et al., 2014; Catalina and Castroviejo, 2017; DeKeyser, 1999; Grove and Jerram, 2011; Martínez-Martínez et al., 2007; Pirard et al., 1999; Russ, 1992). Another significant improvement related to thin section analysis is the development of virtual microscopes for the remote visualization of images. This is possible thanks to the availability of high quality polarized images and software tools for manipulating them (NASA, 2007; Tetley and Daczko, 2014). Another condition for the proper visualization of thin sections in a virtual microscope, other than high quality images of different polarization conditions, is the correct alignment of those images. This technology facilitates the independent viewing of mineral images (thin sections) by large numbers of people in diverse locations (Marcos Pascual, 2014; NASA, 2007; Tetley and Daczko, 2014).

Rock properties can be more thoroughly understood using quantitative information of the petrographic components (minerals, textural characteristics and pore space) obtained by the application of OIA (Asmussen et al., 2015; Higgings, 2006) than using qualitative information only. Quantitative techniques based on digital images of rock thin sections has proved to be paramount in applied geological studies, such as hydrocarbon reservoir characterization (e.g. Du et al., 2018; Ge et al., 2015), aquifer modelling (e.g. Zambrano et al., 2018), or studies seeking the potential CO_2 reservoirs (e.g. Berrezueta and Kovacs, 2017; Lima Neto et al., 2014; Luquot et al., 2016).

☆ Contribution of each author: Edgar Berrezueta conceived, designed and performed the experiments by Optical image analysis. María José Domínguez-Cuesta applied the image corrections by GIS. Ángel Rodríguez-Rey studied thin sections samples and completed the mineralogical study of the samples. All authors wrote the paper and participated in discussion and conclusion of this research article.

* Corresponding author.
E-mail address: e.berrezueta@igme.es (E. Berrezueta).

https://doi.org/10.1016/j.cageo.2018.12.009
Received 15 February 2018; Received in revised form 22 October 2018; Accepted 20 December 2018
Available online 22 December 2018
0098-3004/

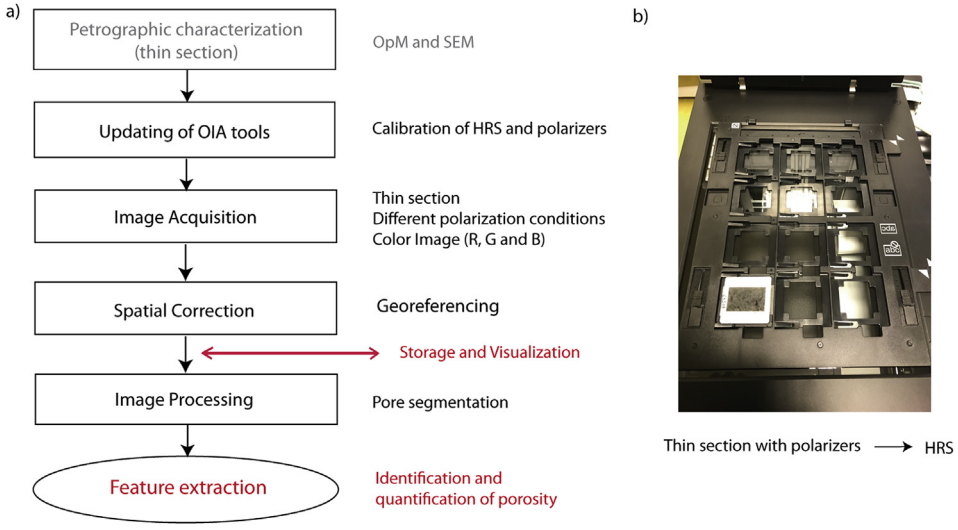

Fig. 1. a) Schematic flowchart of the sequence of pore characterization by OIA-HRS (Modified from González and Woods, 1992; Berrezueta et al., 2017a, b) thin section with polarizers ready for digitalization by means of HRS.

The development of optical systems led to a breakthrough in the manufacture of digital cameras (both photo and video) and high resolution scanners (HRS). The use of digital cameras and HRS in the acquisition of rock images has been widely used in processes based on OIA (e.g. Enrique, 2012; Fueten, 1997; Starkey and Samantaray, 1993; Tarquini and Favalli, 2010). The diverse OIA applications developed to identify petrographic components in two dimensional (2D) images obtained either by optical microscopy (OpM) (e.g. Berrezueta et al., 2015; Borazjani et al., 2016; Fabbri, 1984; Fueten, 1997; Ghiasi-Freez et al., 2009; Sardini et al., 1999; Starkey and Samantaray, 1993; Thompson et al., 2001) or by scanning electron microscopy (SEM) (e.g. Anselmetti et al., 1998; Cipolloni et al., 2014; Arena et al., 2014; Haines et al., 2015) made it possible to greatly improve the performance of the technique offering thus, reproducible and reliable measurements.

According to Anselmetti et al. (1998) and Ehrlich et al. (1984), porosity is, in general, a powerful parameter in rock characterization and its quantification provides valuable insight into the petrography and the physical properties of the rock. Pore space identification and quantification in thin sections by means of OIA is a relatively simple task compared to the study of some other petrographic components (e.g. that of anisotropic minerals with characteristics that vary in accordance with the polarization conditions) (Fueten and Mason, 2001). The use of images of different polarization conditions, as suggested by Fueten (1997) and Thompson et al. (2001), simplifies the identification of mineral phases and, at the same time, offers an optimal and precise method for the identification of the pore space (Berrezueta et al., 2015; Tarquini and Favalli, 2010). Nevertheless, the application of OIA on different images of a petrographic scene requires the correct spatial correlation and registration of the images. According to Tarquini and Favalli (2010), this condition can be achieved by using a proper sample support stage that guarantees the correct alignment during the digitalization of the thin sections. Additionally, corrective steps based on georeferencing are necessary in order to rectify occasional misalignments. Similarly, Berrezueta and Domínguez-Cuesta (2016) addressed the correction of mineral images applying Geographic Information System (GIS) software, in particular, using georeferencing modules (e.g. *QGIS, ArcGIS*). Previous works presented the application of GIS tools to detect grain boundaries in thin sections (Fernández et al., 2012; Li et al., 2008; DeVasto et al., 2012) contributing to quantifying parameters such as shape, orientation and spatial distribution of mineral grains. Furthermore, DeVasto et al. (2012) and Li et al. (2008) included spatial information in the images using GIS, making it possible to relate the parameters measured in the image with real spatial locations at rock massive scale and to conduct detailed spatial analyses. According to Berrezueta et al. (2015), an easy and fast segmentation of the porous system is possible by regions (pixel-based approach), applying the "thresholding" segmentation method (based on threshold values to turn a raw image into a binary one, the pixels being partitioned depending on their intensity value).

In this study, the general procedure of digital image processing (González and Woods, 1992) was applied on thin section images obtained by an HRS, introducing some additional steps for the specific subject of mineral quantification (Berrezueta and Domínguez-Cuesta, 2016; Berrezueta et al., 2017a; DeKeyser, 1999; Pirard et al., 1999; Tarquini and Favalli, 2010). Our aims are i) to describe the procedure of emulating a polarizing microscope by means of an HRS adapted to thin sections study; ii) to provide a detailed protocol for the application of OIA techniques to quantify pore space properties in thin sections; iii) to provide a protocol for the visualization and storage of petrographic images in digital format; and iv) to demonstrate the potential of the proposed system through a case study.

2. Methodology

The sequence of the applied OIA technique is as follows:

i) Mineralogical and petrographic characterization of thin sections by means of qualitative techniques (OpM and SEM observation). The pores were already identified at this stage, in order to help the following OIA quantification process (Fig. 1a).
ii) Set-up and calibration of the OIA equipment (HRS, polarizers, software): color calibration, gain, geometrical calibration (Fig. 1a).
iii) Automation of the image acquisition process on thin sections securing the reproducibility under optimal polarization conditions (Fig. 1 a-b).
iv) Georeferencing sets of images belonging to the same thin section in order to ensure their correct registration (Fig. 1a).
v) Identification of porosity by the application of segmentation ranges to each image.
vi) Quantification of porosity providing pore size and pore shape parameters (area, diameter, perimeter, roundness, and aspect) (Fig. 1a).
vii) Storage of the corrected set of images for their visualization similarly to an optical microscope.

2.1. Techniques

To carry out the mineralogical and petrographic study that formed the basis of the quantification process, an OpM (Leica DM 6000 polarization microscope) and a SEM (JEOL 6100 SEM, using W-Filament, acceleration voltage of 20 kV and *Inca Energy-200 software*) were used. All the experimental runs and studies were performed at the Geological Survey of Spain (Oviedo Unit) and the University of Oviedo (Geology Department).

The HRS that secured the polarization conditions during the image acquisition was an Epson Perfection V850 Pro controlled by a commercial image analysis software (SilverFast SE Plus 8). This device has a resolution of 6400 dots per inch (DPI), which means a real optical resolution of ≈2520 pixels/cm. This scanner uses an Optical Sensor Matrix -charge-coupled device (CCD)- with Micro Lens and High Pass Optics for image digitalization.

The image analysis software managed the digitalization (storing the image in a file) and the conditions of the acquisition (resolution, gain, focus, file format, image compression, etc.). The four polarizing conditions that were used for the digitalization of the thin sections, named 1, 2, 3 and 4, respectively, (crossed polarizers: 90°/0°, 135°/45° and parallel polarizers: 90°/-, 0°/-) (Fig. 2a and b) were obtained by the application of polarizing filters (ST-38-40 Screen Tech). The polarizers were placed under and on top of the sample to achieve crossed-polarized conditions and only on top of the sample to achieve plane-polarized conditions. The set of scanned images (four of them for each petrographic scene) was stored in the Red (R), Green (G) and Blue (B) color system. For each RGB band, 8 bits were used to express color depth (i.e. gray level between 0 and 255). For the spatial correction and the generation of corrected images, a free GIS software (*QGIS* 2.14.0-Essen) was used. The image analysis (segmentation, classification and quantification) of the pore system of a set of corrected digital images (Fig. 2c) was carried out by using an open source image processing system called *ImageJ 1.50i*. All computer programs (SilverFast, ImageJ, QGIS) were run on an IMac I5 with Mountain MacOS X 10.8.

In general, errors during quantification by OIA techniques are similar to those described by Chayes and Faibairn (1951), Demirmen (1971) and Grove and Jerram (2011): (i) using systematic observations for areal analysis (counting error); (ii) variability introduced by the user (operator error); or iii) using 2D sections to estimate vol. % (3D) in hand samples (specimen error). In our study, counting errors on thin sections were not considered because the whole mineral area was studied. According to Grove and Jerram (2011), under similar conditions of analysis by OIA, counted error would be 0.1%. Likewise, specimen error was not assessed because all the quantified parameters were two dimensional. However, specimen variability (Area in 2D) at block sample scale (270 cm^3) was calculated on the studied thin sections due to heterogeneity of material. This specimen variability was calculated on each block sample by studying 5 thin sections for each. The operator errors (e.g. georeferencing process) were calculated by involving five different operators in the measurements on each thin section. Although the study was limited to pore space measurements on the thin section scale, 5 thin sections were measured for each sample (before and after their exposure to SC CO_2) in order to define the mean values and their variation (standard deviation) derived from the characteristics of the rock. The aim of this approach was to provide preliminary information about the variability of the porosity in the studied rock types. In this study, we did not extrapolate values obtained from thin sections to regional scale.

2.2. OIA-HRS process

2.2.1. Updating OIA tools and image acquisition

Thin sections and polarizing filters covering them (both 4.5 cm × 2.8 cm) were placed into a sample support suitable for the HRS (Fig. 1b). This support guaranteed that the samples were close to the same position during measurements under different polarizing conditions and during polarizer replacements. The configuration of illumination properties and thin section optical resolution remained fixed during the digitalization process in order to ensure measurement reproducibility. Thus, with crossed polarizers, gain (1), exposition (100 ms), and tolerance (1) values were used; while, for one polarizer, these values were set to (1), (50 ms) and (1), respectively. One color image (Fig. 3) obtained by digitalizing a thin section by HRS (under polarized conditions) had a size of approximately 150 MB. The time necessary to scan a set of four images was 15 min, in average. Instructions for the acquisition process are illustrated in Fig. 4, in a general manner, and with more detail in Annex 1. Due to the scanning

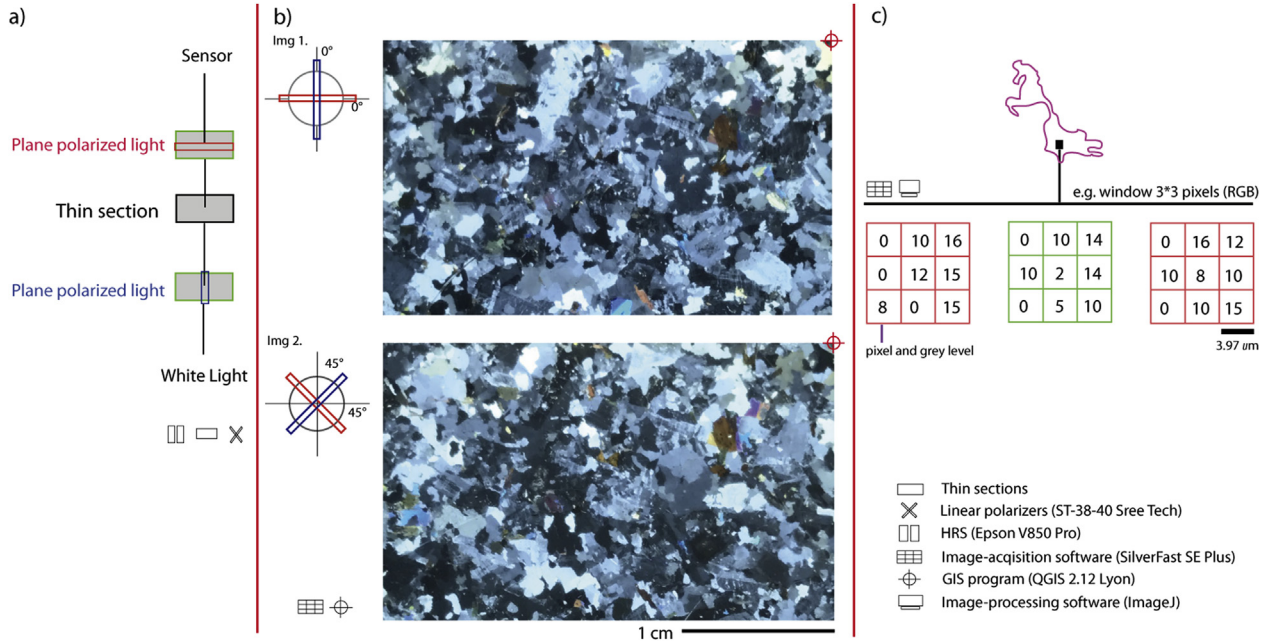

Fig. 2. a) Setting of crossed polarizers in HRS, b) mineral image under cross polarized light acquired in two polarization conditions by HRS, c) digital image of an outlined pore. Modified from Berrezueta et al. (2015).

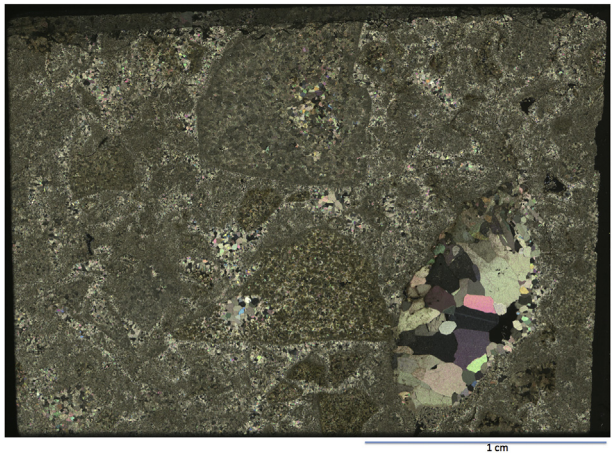

Fig. 3. Example of a scanned thin section (.tiff, 150 MB, 24 bits, RGB color system, 6400 DPI). (For interpretation of the references to color in this figure legend, the reader is referred to the Web version of this article.)

resolution of the scanner (real optical resolution of ≈2520 pixels/cm), the minimum pore size that could be represented in the image was limited to 3.97 μm. The storage of a pixel as a pore occurred if the same pixel (exactly same x and y location) was considered as pore. The digital representation of pores with a size smaller (< 50%) than the minimum detection in the digitalization were not detected or represented during acquisition process.

2.2.2. Spatial correction (georeferencing)

Extracting quantitative information from various images of one petrographic scene (i.e. a thin section) is only possible if the alignment (x and y coordinates) of different mineralogical components (minerals and pores) is certainly the same in the different images (Fig. 5). The process that secures this condition is analogous to that of satellite image correction (Berrezueta et al., 2017a) and it is based on the GIS *QGIS software*. Georeferencing guaranteed that the samples were exactly in the same position during measurements done under different polarizing conditions and during polarizer replacements. In particular, the *Georeferencer* and the *Clipper* tools were used. With the aid of the first one, coordinates were assigned to the mineral images, while the second one was used to crop the referenced images to the same size. The whole process consisted of three general steps: i) a first image was georeferenced by assigning coordinates to three of its corners (Fig. 5a); ii) the rest of the images were referenced by using common points with the first one (Fig. 5b); iii) finally, an area that was common in the corrected images was selected and cropped, and the information was stored in new files (Fig. 5c). The general procedure of the described pre-processing stage (i.e. spatial correction) is presented in Fig. 4b, and it is explained in detail in Annex 2. This stage took approximately 15 min to complete.

2.2.3. Image segmentation and feature extraction

The segmentation process results in the separation of the pore space from the mineral phases of a thin section. Gray level values of pore areas can be calculated by using supervised training steps. The segmentation values defined as ranges for the RGB bands were: i) bands R (0–60), G (0–55) and B (0–65) for crossed-polarized images; and ii) bands R (185–255), G (190–255) and B (160–255) for parallel polarized images. These ranges were determined by the application of sampling windows of 10 × 10 pixels over areas of securely identified pores on the images. The process was repeated for each new sample. The general procedure of pore segmentation using *ImageJ* software is presented in Fig. 6a, while Annex 3 describes the specific procedure applied by the here employed software version. As a result of the intersection of partial segmentations obtained by the *ImageJ software,* the treated area was finally segmented and classified as a pore (Fig. 7).

The classification of a pixel as a pore occurred if the same pixel (exact same x and y location) was considered a pore in all parcial images (GL-ranges within prescribed limits), and the final segmented image resulting from the intersection of partial images. With this process, we secure that pores equal to or greater than 3.97 μm were represented and measured in the images. After their identification by means of generation of binary images (1 for pore and 0 for other phases), the pores can be selected and different parameters of their size and shape can be measured by using the analysis and measurement functions of the software (Annex 3). The principal pore size parameters considered in this study were the area (A), diameter (D), and perimeter (P). Diameter was measured as the diameter of a circle of equivalent area. The principle shape parameters were roundness [1] and aspect [2]. Results of the measurements were saved in .xls files (*Microsoft® Excel®* format). It took approximately 5 min to segment the pores of four images and measure the five parameters.

$$Ro = \frac{4\,\pi\,A}{P^2} \quad [1]$$

$$As = \frac{Major\ Axis}{Minor\ Axis} \quad [2]$$

2.2.4. Storage of images and virtual microscopy

Obtaining digital images of entire thin sections under different polarizing conditions (e.g. 90°/0°; 112.5°/22.5°, 135°/45°, 157.5°/67.5° for crossed nicols and 90°/-; 45°/-; 0°/- for parallel nicols) does not only allow the quantification of mineralogical parameters (e.g. porosity using 90°/0°, 135°/45°, 90°/-; 0°/-), but it also makes it possible to use the digital information in future petrographic studies. For this purpose a virtual microscope was developed, by which the images can be stored and visualized in a computer. The operation of the virtual microscope is based on a video (virtual stack in ImageJ) generated from all the images of a thin section (Fig. 6b). The tool was developed with the Use Virtual Stack option of the ImageJ software applying the following steps (see also Annex 4): a) storing all the images belonging to the same sample in a specific folder; b) renaming each image with a filename that contains a chronologic order (e.g. 01 to 07) of the polarization conditions (e.g. 90°/0° to 0°/-); c) importing the image sequence into imageJ; d) executing the animation (video); and e) saving it in a TIF and an AVI file. The video can be operated by keyboard functions (i.e. start animation by pressing [enter], stop animation by pressing [esc], move backwards and forwards by [<] and [>] keys and also zoom of information by [+] and [-]) or using the ActionBar plugin (Jerome, 2008). The visualization of different images of a same petrographic scene in a video emulates the operation of an optical microscope, since the images represent the changing optical conditions of the mineral phases. However, while under a microscope the optical conditions change due to the rotation of the thin section, here, the position of the thin section is fixed and the polarizer filters are rotated. Another difference lies in the field of visualization area, which is the total sample surface in the case of the digitalized images with the option of zooming in for details thanks to the high digital resolution of the original image.

3. Procedure application in a case study

3.1. Materials

The described procedure has been applied to a study of rocks that can be potentially used for CO_2 geological storage. Pore space properties were compared in samples before and after supercritical (SC) CO_2 exposure in an autoclave. The samples were Jurassic carbonates from the Vasco-Cantabrian basin (Spain). According to García-Lobón et al. (2010), this basin offers ideal conditions for CO_2 storage due to the presence of adequate geological structures, reservoirs and caprocks.

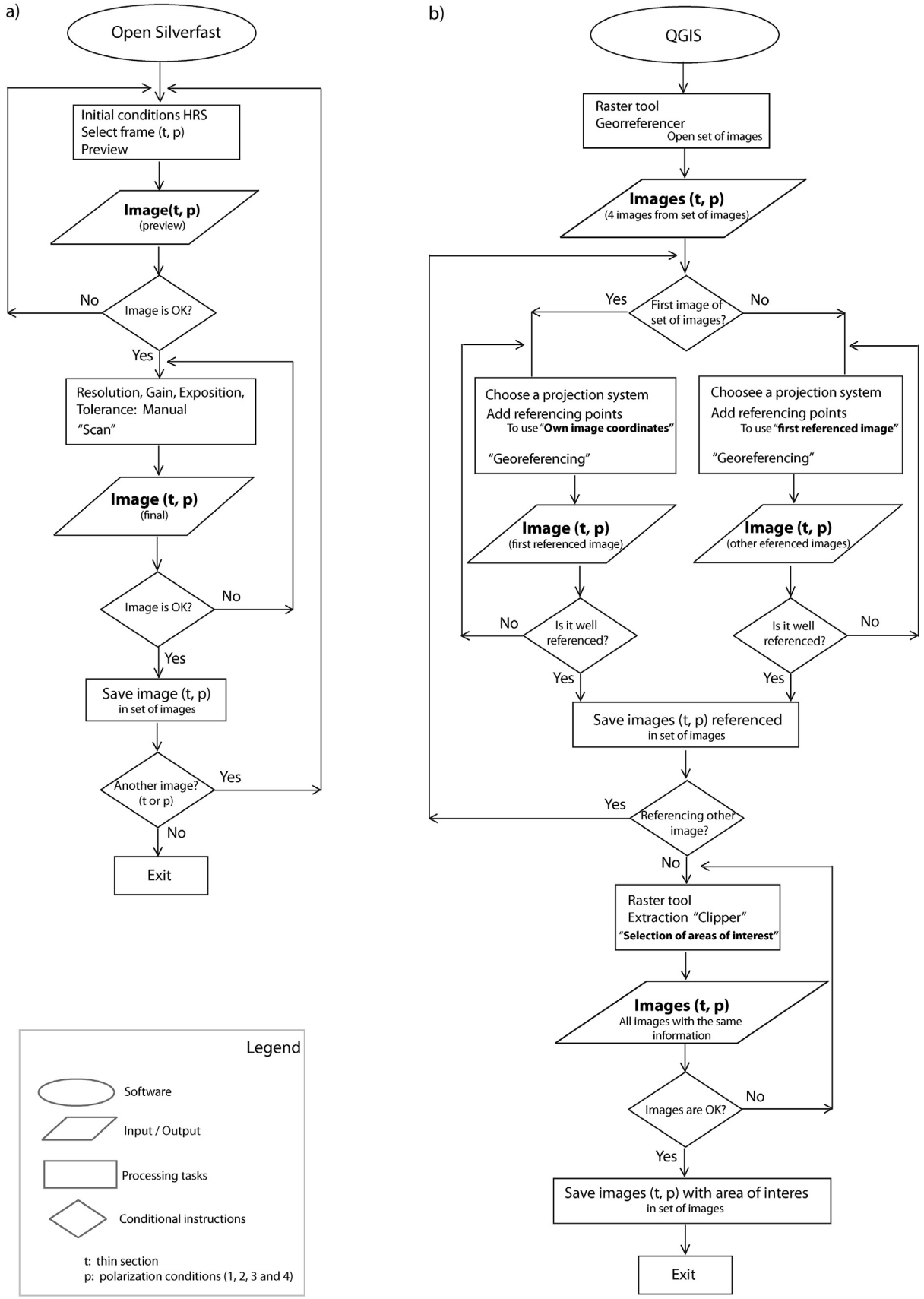

Fig. 4. Schematic workflow: a) acquisition and digitalization of petrographic images using an HRS (Epson V850 Pro) by an image processing software (Silverfast SE Plus 8); b) referencing image set (i.e. a set of images of the same petrographic scene under different polarizing conditions) by means of GIS georeferencing tools (e.g. QGIS 2.14.0-Essen). Polarization conditions 1–4, respectively: 90°/0°, 135°/45° (crossed polarizers) and 90°/-, 0°/- (parallel polarizer).

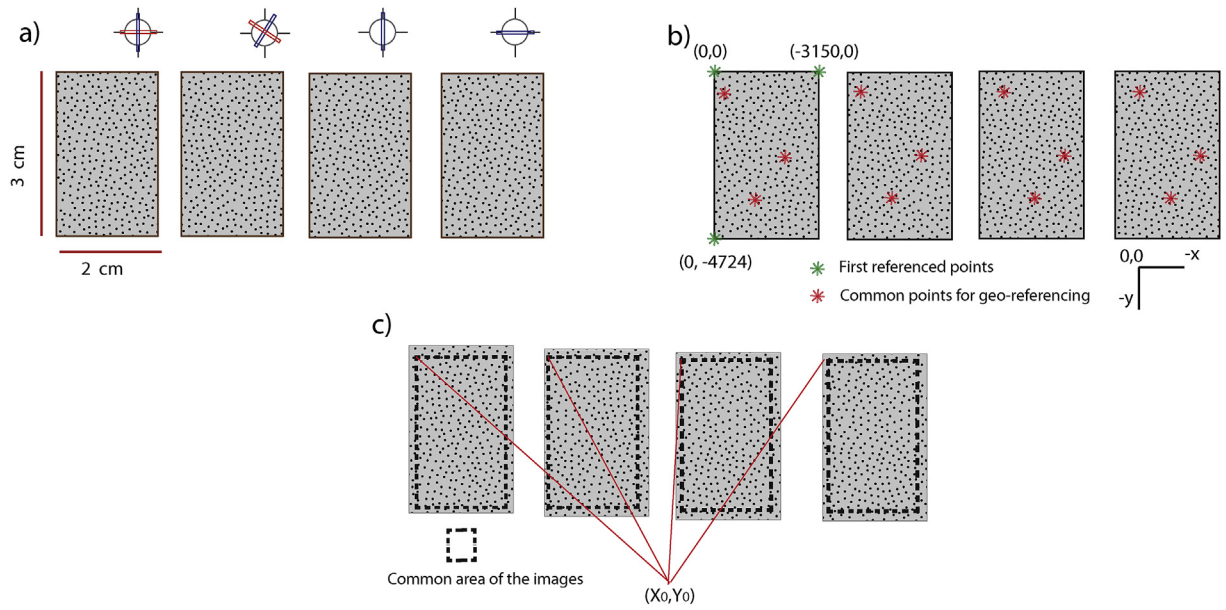

Fig. 5. Referencing mineral images with the use of GIS tools (Berrezueta and Domínguez-Cuesta, 2016; Berrezueta et al., 2017a; Tarquini and Favalli, 2010): (a) image acquisition under polarized light using HRS (two images under cross polarized light and two under parallel polarized light); (b) image georeferencing; (c) selection of areas of interest on a georeferenced image set.

The selected rocks belong to the potential reservoir formations, concretely, they are vuggy carbonates ("Carniolas") of the Puerto de Palombera formation (Hettangian) and oolitic limestones of the Villanueva de Puerta formation (Sinemurian). The vuggy carbonate is a heterogeneous, recrystallized carbonate breccia (calcite and dolomite). Its partial recrystallization resulted in a matrix of highly varying grain size from micrite to crystals up to 200 μm. The angular-subangular clasts are composed of sparite and could be intra-, extra- or bioclasts. This rock shows an open porosity of 4.25%, a connectivity of 3.2 and a permeability-water of 0.752 mD (Mateos-Redondo, 2013). In the oolitic limestone, most of the components (bioclasts, ooids, pellets and matrix) are of calcite composition with scarce presence of dolomite. This rock shows an open porosity of 0.88%, a connectivity of 3.5 and a permeability-gas of 0.002 mD (Mateos-Redondo, 2013).

After field sampling, the material was prepared for SC CO_2 exposure (Fig. 8a) and for petrographic characterization by means of OpM and SEM (Fig. 8b). A previous study of the vuggy carbonates (Berrezueta et al., 2017b) applying OIA-HRS (with scanned images of 4000 DPI) demonstrated changes in the pore space configuration of the sample surfaces due to rock-CO_2 interactions (Fig. 8b).

In this experiment, the vuggy carbonates (135 cm^3) were exposed to brine rich CO_2 (600 cm^3 of brine and 1265 cm^3 of CO_2), while the oolitic limestones (135 cm^3) were exposed to dry CO_2 (1865 cm^3 of CO_2). The pressure (P), temperature (T) and exposure time (t) parameters ($P \approx 7.5$ MPa; $T \approx 35$ °C, and $t = 970$ h, respectively) were selected to simulate the conditions in the vicinity of a theoretical injection well (André et al., 2007). In both cases, it is considered that all the open pores in the evaluated samples were exposed to SC CO_2. The thin sections (four before and four after the experiment) were prepared from areas of the external surface of adjacent carbonate blocks (Fig. 8).

3.2. Pore space quantification

The previous quantitative petrographic study by OpM and SEM (Berrezueta et al., 2017b) demonstrated variations in the pore system of the vuggy carbonates after their exposure to SC CO_2 rich brine. In particular, dissolution textures could be observed including (i) the apparition of secondary pores on the surface of calcite minerals and (ii) a relatively rough surface after CO_2-brine-rock interaction. Quantitatively, porosity increased by 7.77%; roundness decreased by 2.40%, and aspect increased by 2.26%. On the other hand, no alterations were observed in the optical properties of the rock forming minerals on the oolitic limestone after dry SC CO_2 exposure.

Before the quantification and interpretation of the mineralogical parameters by OIA, the variability in the measurements was estimated by using, both the operator and specimen variabilities. The operator variability (Table 1) for the OIA process was tested by 5 different operators (named Operator 1, 2, 3, 4 and 5) and by using 4 test samples (C1_1, C1_CO_2_3, C2_3 and C2_CO_2_1). The total operator variability (operator error) selected was 1.25 (the maximum variability calculated). Furthermore, porosity measurements were made on non-georeferenced image sets. For example, samples C1_1, C1_2, C2_1 and C2_2 show variations of area: 2 to 1 (50% variation between georeferenced images and non-georeferenced images). This variation indicated that the support suitable for HRS did not guarantee the exact same position of the images.

The specimen variability for the samples (two before SC CO_2 and two after SC CO_2) studied by OIA was tested through 5 different thin sections (named Samples 1, 2, 3, 4 and 5) of each sample. The specimen variability (specimen error) is shown in Table 2.

In the present study, the comparative OIA measurements of "before" and "after" samples of the vuggy carbonates and limestones proved that significant changes took place in their porous system. On the thin section scale, variations (Δ: after-before CO_2) of both pore size (porosity in %) and pore shape (Ro and As) parameters were found and quantified (Fig. 9 and Table 3). Optical porosity increased (0.32% for vuggy carbonates and 0.09% for oolitic limestones); roughness decreased (2.40% for vuggy carbonates and 1.13% for oolitic limestones) and pore aspect increased (2.26% for vuggy carbonates and 0.92% for oolitic limestones) after the samples were left to interact with CO_2 (Table 3).

The applied OIA method also provided information about the porosity variation due to sample heterogeneity by comparing different thin sections of the same rock sample (Table 2 and Variation1 (%), in Table 3). Additionally, the variation introduced by the operator ("operator error") was determined, which turned out to be of 1.25% (Table 1 and Variation2 (%), in Table 3).

The comparison of the vuggy carbonate samples before and after their exposure to SC CO_2 revealed an 0.34% absolute increase in

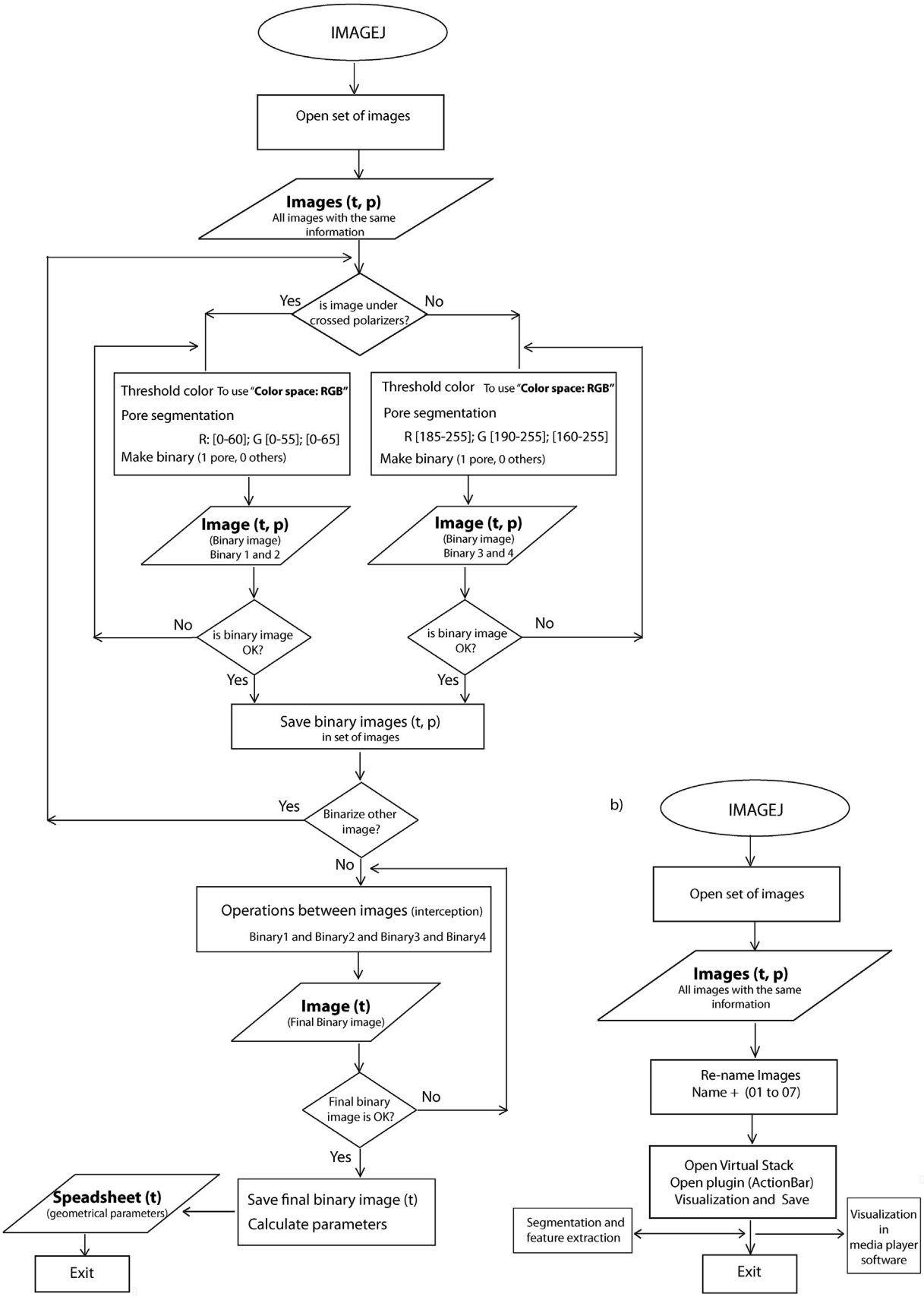

Fig. 6. Schematic general workflow for a) identification and quantification of pores by an OIA program (*ImageJ 1.50i*) and b) visualization of different images with a virtual microscope (*ImageJ 1.50i*).

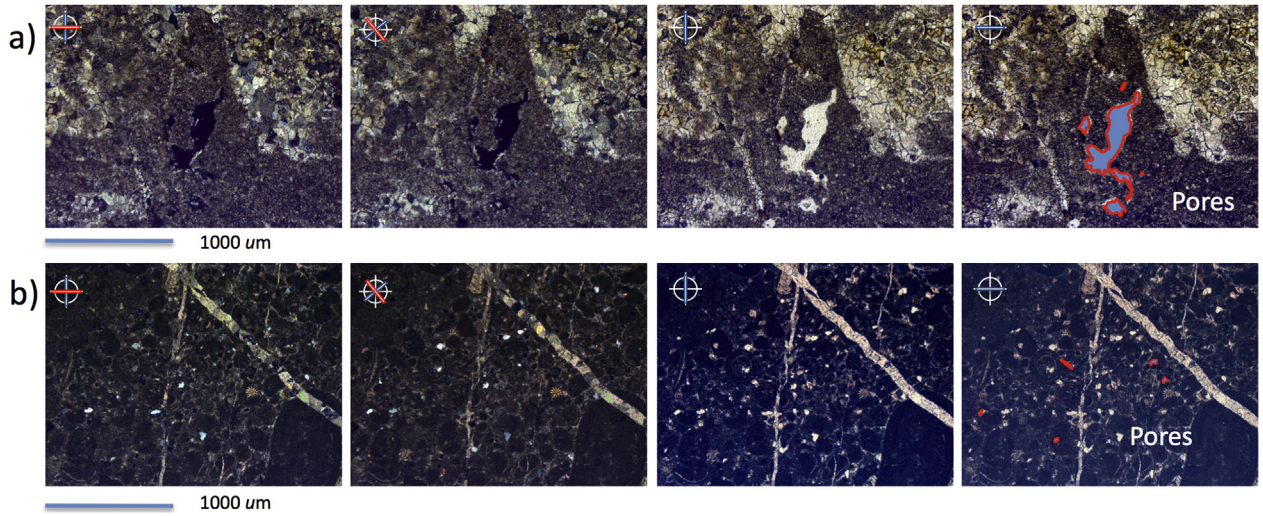

Fig. 7. Image sequence of the same petrographic scene under the four different polarizing conditions used for pore segmentation: a) sample (6 mm^2) of vuggy carbonate and b) sample (6 mm^2) of oolitic limestone.

porosity (that is 8.15%, in relative terms) and, with regard to pore shape, a mean decrease of Ro of 2.24% and a mean increase of As of 1.94%. The comparison of the limestones before and after their exposure to SC CO_2 revealed a 0.09% absolute increase in porosity (that is 5.26%, in relative terms) and, with regard to pore shape, a mean decrease of Ro of 1.13% and a mean increase of As of 0.92%.

3.3. Digital microscopic representation

The digital visualization by ImageJ is presented here through the example of a sandstone sample (Fig. 10). The digital representation of a thin section of 2.5 cm × 1.5 cm through seven images (90°/0°; 112.5°/22.5°; 135°/45°; 157.5°/67.5° for crossed nicols and 90°/-; 45°/-; 0°/- for parallel nicols) occupies approximately 1 GB. The digital files must be properly stored and their order precisely maintained for the correct visualization. Further examples of digital microscopic representation are available in Annex 5.

4. Discussion

4.1. Applicability of method

The process for thin section visualization and pore space quantification presented here was based on the works of DeKeyser (1999), Sardini et al. (1999) and Tarquini and Favalli (2010). These authors quantified mineralogical parameters in thin section images acquired under polarized conditions by HRS. There exist, however, some differences between the aforementioned publications and the approach presented here: i) The use of an *Epson 850 Pro* scanner with an optical resolution of 6400 DPI allowed us to identify and measure objects with sizes of 3.97 μm. This value is significantly higher than optical resolutions obtained in previous studies, such as Sardini et al. (1999) (0.06 mm/pixel, 400 DPI, *Canon CLC 300*), DeKeyser (1999) (9.4 μm/pixel, 2700 DPI, *Nikkon LS-2000*), Tarquini and Favalli (2010) (9.4 μm/pixel,

Table 1
Operator variability (Operator error).

Operator	Sample/Area (%)			
	C1_1	C1_CO_2_3	C2_3	C2_CO_2_1
1	4.08	4.52	1.67	1.82
2	4.28	4.54	1.73	1.77
3	4.19	4.44	1.71	1.79
4	4.14	4.57	1.69	1.81
5	4.16	4.43	1.73	1.80
Average Area	4.16	4.49	1.72	1.80
Operator Variability %	1.25	1.16	1.23	1.07
	1.25			

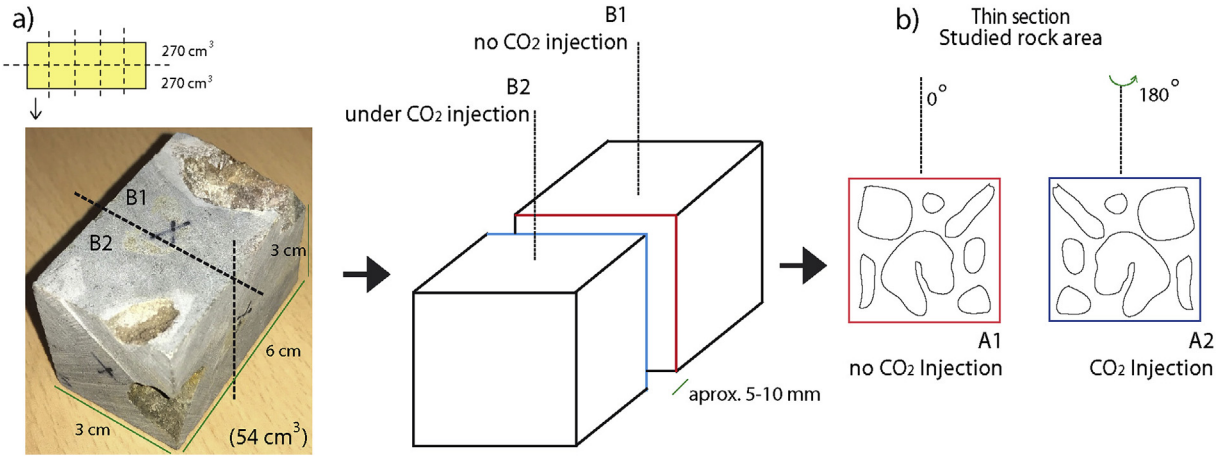

Fig. 8. Schematic representation of the sample preparation sequence (Berrezueta et al., 2017a, 2017b): a) sample blocks (B1 and B2) and b) thin sections of the external surfaces (A1 and A2) of the blocks.

Table 2
Specimen variability (Specimen error) at block sample scale (270 cm^3).

Samples	Area (%)						Specimen Variability %
	1	2	3	4	5	Average Area	
C1	4.16	4.45	4.27	4.07	3.90	4.17	3.65
C1_CO_2	4.56	4.37	4.49	4.92	4.25	4.51	3.82
C2	1.68	1.83	1.72	1.42	1.92	1.71	7.60
C2_CO_2	1.80	1.94	1.82	1.46	2.01	1.80	7.80

2700 DPI, *Nikon Coolscan II*) and Berrezueta et al. (2017a,b) (6.33 μm/pixel, 4000 DPI, *CanonScan FS 4000 US*). This increase in optical resolution is due to the improvements of the used scanner compared to earlier devices. ii) The correct registration of the components of an image set was achieved by georeferencing all of the images by means of GIS. This system has proved to be more precise than processes without image georeferentiation. The registration of images has proved to reduce the variability of measurements (e.g. pore area) from 50% to 1.25% in our tests. Unlike the proposal by Tarquini and Favalli (2010) regarding the use of methods based mainly on a mechanical device with only occasional georeferencing, the systematic use of georeferencing would guarantee a more accurate process. iii) The employed polarizing conditions (90°/0°; 135°/45°; 90°/-; 0°/-) and segmentation ranges (R (0–60), G (0–55), B (0–65) and R (185–255), G (190–255), B (160–255) for crossed and for parallel nicols, respectively) were selected taking into account the results of previous studies (Berrezueta et al., 2015, 2017a). Their use allowed us to accurately identify pores in thin sections. iv) The study was completed applying only free and open-source software (*ImageJ* and *QGIS*) instead of previously used commercial ones (DeVasto et al., 2012; Tarquini and Favalli, 2010). This reduces the expenses and also makes it possible to use and reproduce the applications described here by other researchers. The proposed protocols can also be easily adapted to other GIS and IA software.

In the presented case study, the real optical resolution of the scanner as defined by the manufacturer (6400 DPI) was used as a reference value, and, therefore, 3.97 μm was considered as the minimum detectable pore size. Nevertheless, the users have the liberty to establish other (larger) minimum pore size values that better fit the objectives of their study (e.g. defining the minimum pore size to be considered as 4 pixels (approx. 15.76 μm^2 or of a diameter of approx. 6.32 μm).

Furthermore, the described image acquisition procedure can be extrapolated to any commercial transmitted light scanner independently of its optical resolution, keeping in mind that the measurement range and the image quality are conditioned by the optical resolution.

One of the advantages of OIA studies on thin sections digitalized by HRS – such as the method described here – is the possibility of directly representing the complete surface of a thin section in one single image, which is not possible when using images obtained by CCD cameras coupled to optical microscopes (e.g. Borazjani et al., 2016; Fueten, 1997; Heilbroner, R., 2000). Furthermore, mobile polarizer filters were employed over the thin sections (after Fueten, 1997) in order to obtain images of their entire surface by HRS (DeVasto et al., 2012; Li et al., 2008; Sardini et al., 1999; Tarquini and Favalli, 2010), allowing thus the visualization and identification of mineralogical components emulating an OpM. It takes four times longer to carry out an OIA study of the entire surface of a thin section using low resolution (e.g. 2x) images obtained by an OpM than using polarized images digitalized by an HRS. From the economic point of view, the cost of an OIA-HRS device compared to an OIA-OpM is about 1/10.

It is possible to introduce new polarizing conditions in the image acquisition phase of the described procedure (e.g. 90°/0°; 112.5°/22.5°, 135°/45°, 157.5°/67.5°, 90°/-; 45°/-; 0°/-). Increasing the number of polarizing conditions has principally been applied for mineral phase identification (Fueten, 1997) on images respresenting entire thin sections (DeVasto et al., 2012; Li et al., 2008; Sardini et al., 1999; Tarquini and Favalli, 2010). The same approach was used here i) to store

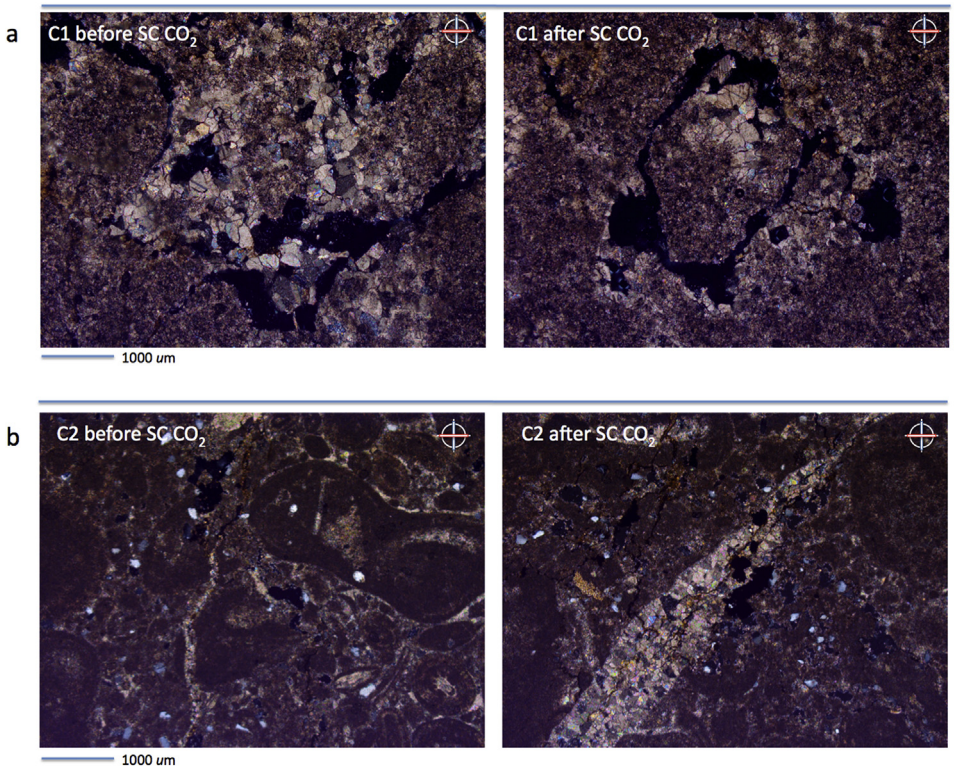

Fig. 9. Comparison of mineral images of a) untreated vuggy carbonates and vuggy carbonates after SC CO_2 exposure, and b) untreated oolitic limestone and oolitic limestone after SC CO_2 exposure.

Table 3
Mean values of Total porosity, Roundness (Ro) and Aspect ratio (As) of carbonate thin sections (before and after SC CO_2 injection) measured by OIA-HRS (6400 DPI). Variation 1 in %: standard deviation/mean of total porosity in 5 samples. Variation 2 in %: standard deviation/mean of total porosity in a same sample measured by 5 different operators. *: Relative variation. Δ: Variation.

Thin sections (number)	Total porosity %	Variation1 % see Table 2	Variation2 % see Table 1	Porosity Change %	Ro	Δ Ro %	As	Δ As %
C1 (5)	4.17	3.65	1.25	0.34	0.630	−2.24	2.212	1.94
C1_CO_2 (5)	4.51	3.82		8.15*	0.615		2.255	
C2 (5)	1.71	7.60		0.09	0.705	−1.13	2.046	0.92
C2_CO_2 (5)	1.80	7.80		5.26*	0.697		2.065	

polarized images of entire thin sections registering mineralogical characteristics with high quality, and ii) to develop a virtual petrographic microscope (Fig. 10). Virtual microscopy contributes to data-sharing and remote access, data-management and annotation and various forms of data-mining (Mikula et al., 2007). It allows both the visualization of global, textural characteristics using images of entire thin sections, as in this study, and more detailed mineralogical observations using images of OpM (e.g. 2x, 10x, 20x) acquired by digital cameras. Nevertheless, a serious limitation in the development of virtual microscopes is posed by the required data size, which often calls for a compromise on quality (image resolution).

4.2. Results, discussion and limitation of the proposed method

The measurements showed up the alterations that took place in the pore system of the vuggy carbonate samples due to rock + CO_2 + brine interactions and which were previously observed by OpM and SEM (Berrezueta et al., 2017b). The results harmonize with chemical and mineralogical processes observed by other authors under similar conditions (André et al., 2007; Kaszuba et al., 2003; Luquot and Gouze, 2009); however, the numerical values (8.15% of porosity change) could be affected by sample variation (3.82% of the porosity) and operator error (1.25%). The comparison of vuggy carbonate samples before and after their exposure to SC CO_2 (Table 3) agrees with the results obtained in a previous study (Berrezueta et al., 2017b), in which 0,32% absolute porosity increase (7.77% in relative terms), 2.40% decrease of Ro and 2.26% increase of As were measured using an OIA-HRS system with a resolution of 4.97 μm/pixel. The difference in the optical resolution of the employed devices (Epson 850 Pro versus Cannon FS 4000 Us) is the principal cause of the deviation in the obtained results since the scanner of the present study (*Epson 850 Pro*) has a resolution that is 62% higher (Haines et al., 2015; Pirard et al., 1999). Nevertheless, it must be pointed out that OIA parameters obtained at different scales are not directly comparable (Berrezueta and Kovacs, 2017; Pirard, 2004). The results must be interpreted within the context of the study and exclusively at the scale applied for the image acquisition.

Based on the literature, the carbonate rocks exposed to dry SC CO_2 (970 h) were not expected to undergo mineralogical or geochemical changes (Berrezueta et al., 2017a,b; Luquot and Gouze, 2009). However, the measurements indicate small variations between the samples

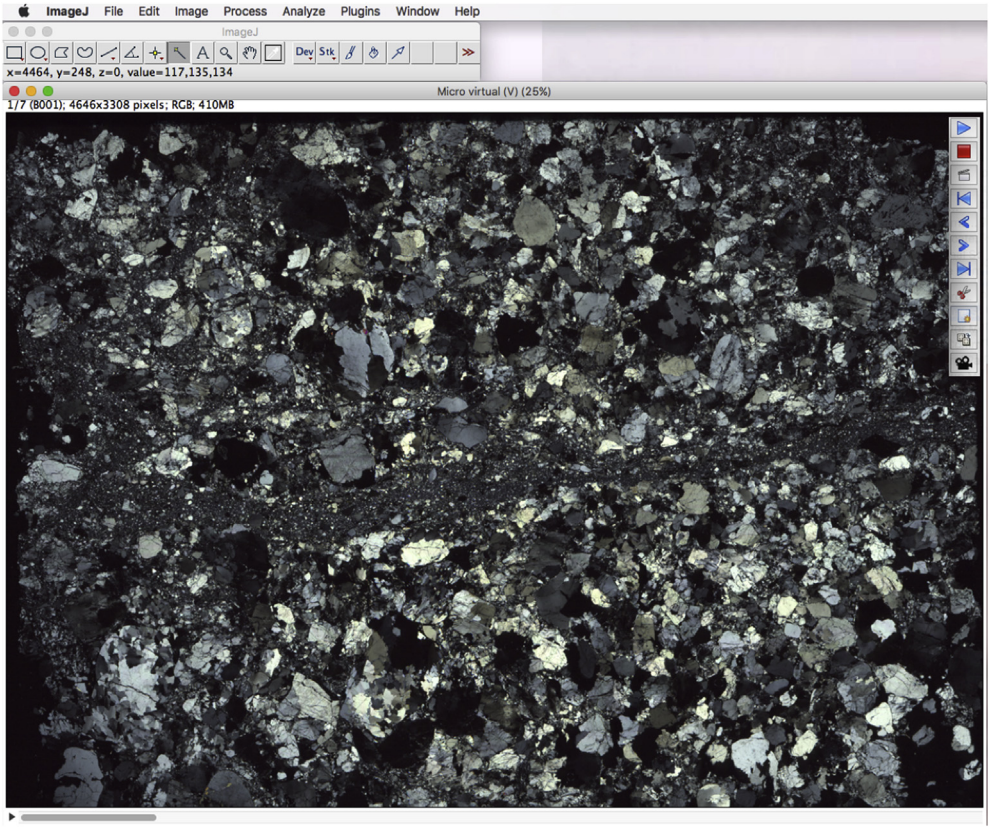

Fig. 10. Example showing the aspect of high resolution mineral images obtained under different polarizing conditions by ImageJ. For more detail and further examples, see Annex 5.

before and after the experiment (Table 3). These changes were not possible to detect by microscopic observations (OpM and SEM), and they might be due to sample variation and operator error (7.8% + 1.25%) and not due to rock-SC CO_2 interaction. Although the porosity parameters calculated on the samples studied by OIA techniques are related to 2D scale, these data provide important information to planning more detailed studies (e.g. 3D modelling).

The success of the method depends on i) properly defining of the image acquisition conditions (eg. resolution of image acquisition), ii) the georeferencing process and iii) the establishment of mineralogical criteria to define the ranges of pore segmentation applicable to the acquired images. The thin section quality is also an important factor that affects the classification process of mineral phases. In order to reduce the influence of the preparation of the samples on the measurements by means of OIA, the same laboratory, the same preparation system and a quality control of the samples should be applied.

According to Pirard et al. (1999) and Berrezueta et al. (2015), the application of OIA requires a rigorous sample preparation protocol, up-to-date OIA tools, and a careful process of image acquisition, segmentation and classification. These altogether will warrant the reproducibility of results.

This explained method could be more efficient by carrying out some improvements as, for example, using a faster and better resolution scanner to reduce the time needed to acquire images and improve their quality. Nevertheless, this semi-automated procedure of digitalization and study of rock thin section has allowed to simplify the study of thin sections.

The technique of presented segmentation (pixel-based classification) was selected due to the easiness to be applied by any user. The limitation (pores misrepresented) of the technique of segmentation (pixel-based approach) used in this work can be solved with the use of object-oriented approach techniques. This method offers a good solution allowing that pixels in close proximity and having similar spectral characteristics are grouped together into a segment. Also segments exhibiting certain shapes, spectral, and spatial characteristics could be grouped into objects. Nowadays some image processing tools are based on methods of pattern recognition and artificial intelligence. The accuracy of the automatic image segmentation methods has been severely compromised by the presence of shared edges of grains, despite the large number of distinct strategies like (a) seed region growing (Choudhury et al., 2006), (b) Level Sets (Lu et al., 2009), partial differential equations (Lu and Ning, 2010), cellular automata (Gorsevski et al., 2012) and image foresting transform (Mingireanov Filho et al., 2013). An adequate choice of the segmentation process is essential to guarantee the correct interpretation of the measures.

5. Conclusions

The application of OIA to evaluate pore space properties of carbonate rocks (thin sections) represents an important advance compared to the traditional petrographic characterization (Figs. 5 and 7). The digitalization of entire thin sections under different polarizing conditions (90°/0°; 135°/45°; 90°/-; 0°/-) with an optimal optical resolution (3.97 μm/pixel) makes it possible to measure petrographic components (i.e. porosity) and their properties of size and shape. Moreover, the application of the proposed procedure is highly facilitated by the use of open source software (*QGIS and Image J*) and by the detailed description of the protocol presented here. A significant improvement of the processing and analysis of microscopic images derives from the application of referencing tools offered by GIS software. The possibility of visualizing a set of images using the OIA software emulating a simplified digital microscope is another important advantage of the present methodology.

The described procedure was successfully applied to a case study of characterizing the evolution of pore space properties of carbonate rocks exposed to SC CO_2.

Acknowledgements

The authors would like to thank the funding provided through the ALGECO2-IRMC Project (Instituto Geológico y Minero de España: 2294-2013). Thanks are due to Cristian Medina (Indiana University Bloomington) providing help in OIA techniques and to Timea Kovacs for her suggestions. We also would like to thank two reviewers (Tiago M. Alves and other anonymous reviewer) for their constructive comments and the editorial office for the editorial handling.

Annexes

Annex 1. Instructions for image acquisition by *SilverFast SE Plus 8I*

1st order	2nd order	3th order
Open SilverFast		
	Start: Silverfast	
	Select information Type (positive)	
		Prescan
		Preview "preliminary scan and selection of area for detailed scan"
		Settings Menu > Exposure Settings "Gain + 1 for polarized images and Gain 0 for non polarized images" Save settings
		Settings Menu > Set Focus "Autofocus"
		Settings Window "configuration as Hi-Res and 24-Bit Color"
		Scann "aprox. 2 min per image"
	File > Save Image (.tif, uncompressed)	
	Exit	

Annex 2. Instructions for spatial correction of images by *QGIS 2,14,0-Essen*

1st order	2nd order	3th order
Open QGIS		
	Open New Project	
	Raster > Georeferencer > **Georeferencer** "to open the plugin".	
		Open Raster "Image 1 and + proj = longlat + datum = WGS84"
		Add Point "Enter coordinates from information of the same image x-y pixels"
		Start georeferencing "Polinomyal 1, closest neighbor"
		Save Image "1 geo-ref, .tif"
		"Open next image"

		Open raster “Images 2 to 4 + proj = longlat + datum = WGS84″ Add Point “Enter coordinates from previous Image geo-referenced” Start georeferencing Save Image “2 to 4 geo-ref, .tif ”
	Close Georeferencer Raster > Extraction > **Clipper** “Selection of areas of interest”	
		File > Save Images
	Close Clipper Save Project Exit	

Annex 3. Instructions for image segmentation and measurement by *ImageJ 1.50i.*

1st order	2nd order	3th order
Open ImageJ		
	File > Open > .tif “to open georeferenced image from image set”. Image > Adjust > Color Threshold > “window threshold is displayed”	

		Thresholding method > Default “selection of method”
		Threshold color > Red “selection will be shown red”
		Color space > RGB “system used for segmentation”
		Select segmentation ranges in histograms >
		If image is in cross polarized light then
		R: [0–60]; G [0–55]; [0–65]
		If image is in plane polarized light then
		R [185–255]; G [190–255]; [160–255]
		Select > “partial binary image is generated”

	Process > Binary > Make Binary	
		File > Save as > .tif “to save partial binary image”.
	Go to File Open until open all images “all images of image set” Process > Image Calculator > “window image calculator is displayed”	
		Binary1 and Binary2 and Binary3 and Binary4 “They are intercepted –and operator- to generate final binary image” File > Save as > .tif “to save final binary image”.
	Analyze > Set Measurements > “window set measurement is displayed” Analyze > Analyze Particles > “window analyze particles is displayed “	Parameters: A, P, D, Axis. Ro, As
		File > Save Results and Summary “.xls format”
	Exit	

Annex 4. Instructions for image visualization by virtual microscope in *ImageJ 1.50i.*

1st order	2nd order	3th order
Open ImageJ		
	File > Open > .tif “to open georeferenced images from image set”. Image > Type > Stacks > Images to Stack > “Stack of images” Image > File > Save as > Image Sequence “Sequence in .tif”	
		Import pluging: Action bar
	Image > File > Save as > Image Sequence “Sequence in .AVI″ Exit	

6. Annex 5

https://drive.google.com/open?id=1uIUjW8uwEXfwwPM-5D-UiNL9H2sEA1sO.

References

André, L., Audigane, P., Azaroual, M., Menjoz, A., 2007. Numerical modelling of fluid-rock chemical interactions at the supercritical CO_2-liquid interface during CO_2 injection into a carbonate reservoir, the Dogger aquifer (Paris Basin, France). Energy Convers. Manag. 48, 1782–1797.

Anselmetti, F., Luthi, S., Eberli, G.P., 1998. Quantitative characterization of carbonate pore systems by digital image analysis. AAPG Bull. 82 (10), 1815–1836.

Arena, A., Delle Piane, C., Sarout, J., 2014. A new computational approach to cracks quantification from 2D image analysis: application to micro-cracks description in rocks. Comput. Geosci. 66, 106–120.

Asmussen, P., Conrad, O., Günter, A., Kirsch, M., Riller, U., 2015. Semi-automatic segmentation of petrographic thin section images using a "seeded-region growing algorithm" with as application to characterize weathered subarkose sandstone. Comput. Geosci. 83, 89–99.

Berrezueta, E., González-Menéndez, L., Ordoñez-Casado, B., Olaya, P., 2015. Pore network quantification of sandstones under experimental CO_2 injection using Image Analysis. Comput. Geosci. 77, 97–110.

Berrezueta, E., Domínguez-Cuesta, M.J., 2016. Quantification of sandstone pore system

by optical image analysis through high-resolution scanner images. In: Proceedings of IX Congreso Geológico de España, Huelva, Spain, pp. 1–4 on CD-ROM.
Berrezueta, E., Kovacs, T., 2017. Application of optical image analysis to the assessment of pore space evolution after CO_2 injection in sandstones. A case study. J. Petrol. Sci. Eng. 159, 679–690.
Berrezueta, E., Domínguez-Cuesta, M.J., Ordóñez-Casado, B., Medina, C., Molinero, R., 2017a. Pore space quantification of sedimentary rocks before-after supercritical CO_2 interaction by optical image analysis. Energy Procedia 114, 4382–4393.
Berrezueta, E., Kovacs, T., Luquot, L., 2017b. Qualitative and quantitative changes of carbonate rocks exposed to SC CO_2 (Basque-Cantabrian basin, Northern Spain). Appl. Sci. 7 (11), e1124.
Borazjani, O., Ghiasi-Freez, J., Hatampour, A., 2016. Two intelligent pattern recognition models for automatic identification of textural and pore space characteristics of the carbonate reservoir rocks using thin section images. J. Nat. Gas Sci. Eng. 35 (A), 944–955.
Catalina, J.C., Castroviejo, R., 2017. Microscopía de reflectancia multiespectral: aplicación al reconocimiento automatizado de menas metálicas. Rev. Métall. 53 (4), e107.
Chayes, F., Fairbairn, H., 1951. A test of the precision of thin section analysis by point counter. Am. Mineral. 34, 1–11.
Choudhury, K.R., Meere, P.A., Mulchrone, K.F., 2006. Automated grain boundary detection by CASRG. J. Struct. Geol. 28, 363–375.
Cipolloni, G., Menapace, C., Cristofolini, I., Molinari, A., 2014. A quantitative characterization of porosity in a Cr-Mo sintered steel using image analysis. Mater. Char. 94, 58–68.
DeKeyser, T.L., 1999. Digital scanning of thin sections and peels. J. Sed. Research 69 (4), 964 964.
Demirmen, F., 1971. Counting error in petrographic point-count analysis: a theorical and experimental study. Math. Geol. 3 (1), 15–41.
DeVasto, M.A., Czeck, D.M., Bhattacharyya, P., 2012. Using image analysis and ArcGIS to improve automatic grain boundary detection and quantify geological images. Comput. Geosci. 49, 38–45.
Du, S., Pang, S., Shi, Y., 2018. A new and more precise experiment method for characterizing the mineralogical heterogeneity of unconventional hydrocarbon reservoirs. Fuel 232, 666–671.
Ehrlich, R., Crabtree, S.J., Kennedy, S.K., Cannon, R.L., 1984. Petrographic image analysis I: analyses of reservoir pore complexes. J. Sediment. Petrol. 54, 1365–1378.
Enrique, P., 2012. Petrografía de rocas ígneas y metamórficas a bajo aumento mediante el uso del escáner de transparencias. Geogaceta 51, 7–10.
Fabbri, A.G., 1984. Image Processing of Geological Data. Van Nostrand-Reinhold, Wokingham, UK, pp. 224.
Fernández, F.J., Menéndez-Duarte, R., Aller, J., Bastida, F., 2012. Application of geographic information system to shape-fabric analysis. In: Microstructural evolution and physical properties in high-strain zones, vol. 245. pp. 409–420.
Fueten, F., 1997. A computer-controlled rotating polarizer stage for the petrographic microscope. Comput. Geosci. 23 (2), 203–208.
Fueten, F., Mason, J., 2001. An artificial neural net assisted approach to editing edges in petrographic images collected with rotating polarizer stage. Comput. Geosci. 33 (9), 1176–1188.
Ge, X., Fan, Y., Li, J., Aleem Zahid, M., 2015. Pore structure characterization and classification using multifractal theory-an application in santanghu basin of western China. J. Petrol. Sci. Eng. 127, 297–304.
García-Lobón, J.L., Reguera-García, M.I., Martín-León, J., Rey-Moral, C., Berrezueta, E., 2010. Plan de selección y caracterización de áreas y estructuras favorables para el almacenamiento geológico de CO_2 en España. Resumen ejecutivo. Instituto Geológico y Minero de España, pp. 75.
Ghiasi-Freez, J., Soleimanpour, I., Kadkhodaie-Llkhchi, A., Ziaii, M., Sedighi, M., Hatampour, A., 2009. Semi-automated porosity identification from thin section images using image analysis and intelligent discriminant classifiers. Comput. Geosci. 45, 36–45.
González, R.C., Woods, R.C., 1992. Digital Image Processing. Addison-Wesley Publishing Co., New York, pp. 716.
Gorsevski, P.V., Onasch, C.M., Farver, J.R., Ye, X., 2012. Detecting grain boundaries in deformed Rocks using a cellular automata approach. Comput. Geosci. 42, 136–142.
Grove, C., Jerram, D.A., 2011. jPOR: an ImageJ macro to quantify total optical porosity from blue-stained thin sections. Comput. Geosci. 37 (11), 1850–1859.
Haines, T., Neilson, J.E., Healy, D., Michie, E., 2015. The impact of carbonate texture on the quantification of total porosity by image analysis. Comput. Geosci. 85, 112–125.
Heilbroner, R., 2000. Automatic grain boundary detection and grain size analysis using polarization micrographs or orientation images. J. Struct. Geol. 22, 969–981.
Higgings, M.D., 2006. Quantitative Textural Measurements in Igneous and Metamorphic Rocks. Cambrigde University Press, Cambrigde (UK), pp. 265.
Jerome, M., 2008. Custom toolbars and mini applications with Action bar. In: Proceedings of ImageJ User and Developer Conference, Luxembourg, Luxembourg, pp. 1–7. https://dx.doi.org/10.6084/m9.figshare.3397603.v3.
Kaszuba, J.P., Janecky, D.R., Snow, M.G., 2003. Carbon dioxide reaction processes in a model brine aquifer at 200∘C and 200 bars: implications for geologic sequestration of carbon. Appl. Geochem. 18, 1065–1080.
Li, Y., Onasch, C.M., Guo, Y., 2008. GIS-based detection of grain boundaries. J. Struct. Geol. 30, 431–443.
Lima Neto, I., Misságia, Ceia, M., Archilha, N., Oliveira, L., 2014. Carbonate pore system evaluation using the velocity-porosity-pressure relationship, digital image analysis, and differential effective medium theory. J. Appl. Geophys. 110, 23–33.
Lu, B., Cui, M., Liu, Q., Wang, Y., 2009. Automated grain boundary detection using the level set method. Comput. Geosci. 35, 267–275.
Lu, B., Ning, C., 2010. PDE-based grain boundary detection. In: Proceedings of the Second IITA International Conference on Geoscience and Remote Sensing, vol. 2. pp. 170–173.
Luquot, L., Gouze, P., 2009. Experimental determination of porosity and permeability changes induced by injection of CO_2 into carbonate Rocks. Chem. Geol. 265, 148–159.
Luquot, L., Herbert, V., Rodriguez, O., 2016. Calculating structural and geometrical parameters by laboratory measurements and X-ray microtomography: a comparative study applied to a limestone sample before and after a dissolution experiment. Solid Earth 7, 441–456.
Marcos Pascual, C., 2014. Microscopio virtual de luz polarizada. Campus virtual de la Universidad de Oviedo. Available at: http://ocw.uniovi.es/pluginfile.php/4552/mod_resource/content/41/microscopio/index.html.
Martínez-Martínez, J., Benavente, D., García del Cura, M.A., 2007. Petrographic quantification of brecciated Rocks by image analysis. Application to the interpretation of elastic wave velocities. J. Eng. Geol. 90, 41–54.
Mateos-Redondo, F., 2013. Caracterización de las rocas jurásicas-cretácicas correspondientes a las rocas almacén y sello presentes en la estructura geológica de Hontomín: Planta de desarrollo tecnológico de almacenamiento geológico de CO2. Technical report. pp. 90.
Mikula, S., Trotts, I., Stone, J.M., Jones, E.G., 2007. Internet-enabled high-resolution brain mapping and virtual microscopy. Neuroimage 35 (1), 9–15.
Mingireanov Filho, I., Spina, T.V., Falcão, A.X., Vidal, A.C., 2013. Segmentation of sandstone thin section images with separation of touching grains using optimum path forest operators. Comput. Geosci. 57, 147–157.
NASA, 2007. Virtual microscope. 2007. Available at: http://virtual.itg.uiuc.edu/.
Pirard, E., Lebrun, V., Nivart, J.F., 1999. Optimal image acquisition of video images of reflected light. Eur. Microsc. Anal. 60, 9–11.
Pirard, E., 2004. Multispectral imaging of ore minerals in optical microscopy. Mineral. Mag. 68 (2), 223–233.
Russ, J.C., 1992. The Image Processing Handbook. CRC Press, Boca Raton, FL, pp. 444.
Sardini, P., Moreau, E., Sammartino, S., Touchard, G., 1999. Primary mineral connectivity of polyphasic igneous rocks by high-quality digitization and 2D image analysis. Comput. Geosci. 25, 599–608.
Starkey, J., Samantaray, A.K., 1993. Edge detection in petrographic images. J. Microsc. 172 (3), 263–266.
Tarquini, S., Favalli, M.A., 2010. Microscopic information system (MIS) for petrographic analysis. Comput. Geosci. 36, 665–674.
Tetley, M.G., Daczko, N.R., 2014. Virtual Petrographic Microscope: a multi-platform education and research software tool to analyses rock thin-sections. Aust. J. Earth Sci. 61 (4), 1–7.
Thompson, S., Fueten, F., Bockus, D., 2001. Mineral identification using artificial neural network and the rotating polarizer stage. Comput. Geosci. 27, 1081–1089.
Zambrano, M., Tondi, E., Mancini, L., Lanzafame, G., Trias, F.X., Arzilli, F., Materazzi, M., Torrieri, S., 2018. Fluid flow simulation and permeability computation in deformed porous carbonate grainstones. Adv. Water Resour. 115, 95–111.